Energy & Buildings 346 (2025) 116235

Contents lists available at ScienceDirect

Energy & Buildings

journal homepage: www.elsevier.com/locate/enb

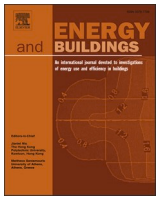

Impact of Building-Grid interaction signals on energy flexibility at cluster Level: Insights from two case studies

Tuğçin Kırant-Mitić [a,*], Monika Hall [b], George Dawes [c], Rui Amaral Lopes [d]

[a] Department of Building Physics and Technical Services, Faculty of Architecture and Civil Engineering, Wuppertal University, Wuppertal, Germany
[b] Institute of Sustainability and Energy in Construction, University of Applied Sciences and Arts Northwestern Switzerland, Muttenz, Switzerland
[c] Building Energy Research Group (BERG), Department of Architecture, Building and Civil Engineering, Loughborough University, Loughborough LE11 3UE, UK
[d] School of Science and Technology, UNINOVA-CTS and LASI, NOVA University Lisbon, Portugal

ARTICLE INFO

Keywords:
Building-Grid Interaction Signal
Transformer Aging
Building Energy Flexibility
Building Cluster

ABSTRACT

The increasing integration of renewable energy sources into power grids introduces operational challenges due to their time-varying electricity supply and limited predictability. Building-grid interaction (BGI) signals have emerged as a strategy to enhance energy flexibility, yet their impact on distribution transformer performance and aging remains underexplored. This study investigates the role of single vs. sequential BGI signals in two energy-efficient building clusters in Germany and Switzerland, using a co-simulation framework that integrates building performance simulation tools with numerical computing methods. Single BGI signals, such as electricity price and CO_2eq intensity, were compared to sequential BGI signals, which incorporate a transformer critical status signal to dynamically adjust flexibility responses. The results reveal distinct impacts on transformer aging and grid stress between the two clusters. In the German building cluster, sequential BGI signals effectively mitigated demand-driven transformer stress, reducing aging compared to single-signal cases, which impacted peak loads. Conversely, in the Swiss building cluster, photovoltaic feed-in was the dominant aging factor. Here, single BGI signals slightly lowered aging through improved self-consumption, while transformer critical status signals occasionally increased aging by reducing self-consumption during overload events. Across both clusters, energy and cost savings were analysed, with building-grid interaction signal integration successfully maintaining thermal comfort boundaries. These findings provide insights for energy flexibility aggregators on the potential trade-offs between grid stability, economic efficiency, and emission reductions in flexible building operations.

1. Introduction

In response to the global challenge of climate change, many nations have committed to achieving net-zero carbon emissions by 2050 [1]. A key strategy in this effort is the widespread deployment of renewable energy systems (RES) to decarbonise the power grid. However, as nations transition from traditional high inertia-based power generation to time-varying, low-inertia power generation from RES, they face significant operational challenges. Renewable energy sources, such as wind and photovoltaic (PV), are inherently variable, making it challenging to reliably predict power generation levels [2]. Such variability in energy supply can create stability issues for the power grid, particularly as RES penetration increases. To address these challenges, a whole-systems approach is required – one which incorporates the building sector as part of the solution. Building services, including heating, ventilation, and air conditioning (HVAC), thermal storage, energy generation, electrical storage systems and building automation systems, play a crucial role in this integration [3,4]. Building grid interaction (BGI) can be used to provide advanced services such as demand-side management (DSM). As the demand for electricity in buildings grows, driven by increased use of heat pumps and electric vehicles, the mismatch between renewable generation and consumption peaks becomes more pronounced.

The current power distribution networks were not designed to accommodate the energy transition [5], and their capacity may not be sufficient to meet the needs of widespread electrification as a major overload situation may occur for the distribution transformer [6]. For instance, full electrification of heating systems could increase peak electricity demand by 170 %, necessitating a 160 % expansion of grid capacity in the UK [7]. Besides, traditional power grids operate using a

* Corresponding author.
E-mail address: tugcin.kirant_mitic@uni-wuppertal.de (T. Kırant-Mitić).

https://doi.org/10.1016/j.enbuild.2025.116235
Received 4 May 2025; Received in revised form 7 July 2025; Accepted 30 July 2025
Available online 2 August 2025

top-down approach, with one-way power flows from centralised generators to consumers [8]. However, the rise of decentralised energy sources, like rooftop PV, has introduced bidirectional flow [9], requiring a transition to smart grid systems for improved flexibility and resilience. Smart grids facilitate a high level of coordination between buildings and the power grid enabling more efficient energy management [10]. Utilising the information provided by smart grid systems through a control signal, the interaction between a building and the power grid can be exploited for operational optimisation [11]. BGI goals are linked to the optimisation or operational objectives of smart grid systems [12] such as frequency regulation [13] and voltage control to prevent fluctuations and maintain a reliable power supply [14]. Pricing also plays a crucial role, such as dynamic pricing schemes incentivise consumers to change their energy use during peak periods [15]. Furthermore, emissions-based signals encourage energy use when grid emissions are at their lowest, or when the supply of renewable energy is plentiful, thereby contributing to the decrease of greenhouse gas (GHG) emissions [16]. Load-based flexibility also features through programs for demand response and load-shifting, which serve to alleviate grid strain by modifying consumption during peak times, thereby enhancing stability.

On the other side, the effectiveness of these signals depends on their ability to transparently convey the value of flexibility to end-users. For instance, using a single control signal across a cluster of buildings can lead to unintended consequences. If all buildings respond to the same signal simultaneously, such as a favourable electricity price, this synchronised behaviour can overload the grid and cause congestion [17,18], bringing adverse peak-shifts and rebound peaks [19], which can destabilise the power grid. There is a positive motivation behind using a single signal, but it may lead to operational drawbacks, including distribution transformer overutilisation and accelerated aging, which can compromise the overall efficiency and reliability of power grid operation.

Existing BGI studies focus on single control signals such as price and CO_2 [19,20] but overlook their impact on transformer stress and aging. Research on optimized signals has improved joint influence of different single signals as price and CO_2, but lacks real-time power grid responsiveness [21]. [22] showed different agent functions such as price and grid stress signal from a peer-to-peer platform. By cooperating two different signals, the grid stability is always controlled while aiming cost effective operation. Similarly, [23] introduced a genetic algorithm-based flexibility optimization model, balancing grid stability and financial incentives. This approach optimizes electrical vehicle charging flexibility to reduce congestion costs. While they effectively reduce short-term costs and congestion, they do not incorporate transformer operational status. [24] developed a transformer model to assess aging impacts under varying load conditions, but their analysis was limited to signal-unaware demand scenarios. A more transformer-aware flexibility model was presented by [25], who developed a multi-stage optimization framework integrating home energy management systems and peer-to-peer trading. Their approach ensures grid-friendly flexibility activation by imposing transformer overload risk limits; however, their control approach does not include immediate operational changes to avoid transformer overload.

To this end, introducing additional signals is necessary to overcome operational challenges and ensure stable grid operation. Despite significant advancements in BGI research, several critical gaps remain:

- Priority between objectives: Current studies lack a systematic analysis for quantifying the relative impact of signals −such as cost and grid stability- within control strategies.
- Localized grid constraints: Grid-level impacts, such as distribution transformer operation status as overloading and fastened aging, are underexplored under dynamic signal scenarios.
- Sequential signal operation: Few studies have evaluated the effectiveness of sequential signals in mitigating transformer overload while maintaining BGI operation.
- Heterogeneity in building clusters: Most research focuses on one building cluster, failing to address the diverse properties and behaviours of different clusters.

Tackling these challenges, this study aims to examine the impacts of control signals on building clusters and power grid operation, by comparing the effects of single versus sequential penalty signals on distribution transformer performance and lifespan; a novel contribution to the field, as this is a previously underexplored aspect with significant implications to both the buildings, power grid networks and their interactions. However, the term “penalty signal” may carry negative connotations, making it less effective for engaging stakeholders, particularly in commercial contexts [26]. To address this, we propose the term “building-grid interaction signal” (BGI signal). A BGI signal is defined as “a dynamic signal that prompts adjustments in a building’s systems or services to align with operational goals and external factors such as grid service requirements”. Unlike penalty signals, BGI signals are not restricted to cost-specific factors and can encompass multiple control variables, offering a more inclusive and stakeholder-friendly approach to demand response initiatives. The literature outlines several types of BGI signals that can be applied to buildings:

1 Single BGI signal

A single signal is employed to achieve or optimise for a specific objective, such as minimising energy costs or reducing GHG emission [20,27]. This approach is straightforward, as it focuses on one parameter without accounting for trade-offs with other objectives.

2 Optimised or Compound BGI signal

Multiple parameters are simultaneously considered within a single signal, enabling a balance between objectives such as energy costs and GHG emission saving [28,29]. This requires pre-processing to generate a combined BGI signal at each time step. The process often involves a decision tree or weighted balancing method, where weights are assigned based on the importance of each parameter or the overall optimisation objective. This type of signal is particularly suited to scenarios where trade-offs between competing objectives must be resolved dynamically.

3 Sequential BGI signal

Multiple signals are applied concurrently, but only one signal is active at any given moment, based on a predefined priority hierarchy. For example, a baseline signal might optimise energy costs to minimise operational expenses. However, if a critical event occurs – such as power instability – a higher-priority signal is activated to address the urgent need for demand change. During this period, the priority signal temporarily overrides the baseline signal to tackle the greater issue. Once the issue is resolved, the system reverts to the baseline optimisation signal.

Sequential signals directly address the localized constraints by incorporating real-time feedback from grid infrastructure, such as transformer load and hot spot temperature (HST). However, the studies evaluating their impact on grid operations, particularly in the context of transformer aging, are limited. The integration of dynamic BGI signals into such models remains an open research question. This study focuses on these gaps by:

– Developing a co-simulation framework to evaluate the impacts of sequential BGI signals on building clusters and power grid operations.

Building performance simulations (BPS) are conducted in a co-simulation environment to analyse the use of *single signals* such as electricity unit price and power grid electricity carbon dioxide equivalent (CO_2eq) intensity in BGI operation, focusing on building clusters from Germany and Switzerland.

– Quantifying transformer aging and HST fluctuations under dynamic signal scenarios using sequential signals.

After performing the simulations using a *single signal*, further simulations were performed using a *sequential signal* arrangement; considering a single signal alongside a transformer critical status (TCS) signal, to evaluate the impacts that multiple signals (two signals are applied in the scope of this research) can have on flexibility objectives and grid

stability across building clusters. The distribution transformer model, which was used to create the TCS signal and calculate transformer aging, complies with the principles specified in the IEC 60076–7 standard [30]. Consequently, the distribution transformer load, energy costs, GHG emissions, distribution transformer aging and the indoor thermal comfort results are presented in this research.

The paper is structured as follows: Section 2 introduces the methodology, including the two investigated building clusters, a description of the signals used, and the numerical setup. In Section 3, the results of cluster and distribution transformer operation based on different signals are presented. Section 4 examines the context of different building cluster analysis, concluding with this study's key findings and outlining directions for future work.

2. Methodology

This research analyses two building clusters located in Germany and Switzerland as part of the IEA EBC Annex 82 – Energy Flexible Buildings Towards Resilient Low Carbon Energy Systems framework, which involves researchers from multiple institutions. The distinct characteristics of the case study areas, including country-specific standards, regulations, and operational practices, necessitated the application of different methodologies. Additionally, the institutions conducting the research employed varied BPS tools and numerical methods, reflecting their approaches. These differences, while inherent to international collaborations, contribute to a broader understanding of BGI by showcasing diverse strategies for building operations and control. The presented work represents a unified effort to address these variations and integrate insights from different contexts. This research does not aim to directly compare the clusters but rather to analyse them independently to understand how BGI signals function in distinct operational settings. The description of the clusters, BGI signal used, simulation cases, applied control strategies and numerical setup of co-simulation environments are described in the following section.

2.1. Cluster definition – Wuppertal, Germany

As part of the Solar Decathlon Europe 21/22 competition, which was organised in Wuppertal, Germany, 18 teams designed and built energy-efficient solar powered houses [31]. For further research activities to be conducted under the "Living Lab NRW" project, eight of these buildings remained in Wuppertal (Fig. 1). Wuppertal's climate is characterised by moderate winters and summers, with a long-term mean annual temperature of 10.5 °C and a total global solar radiation of 942 kWh/m^2 per year [32].

The buildings in the cluster were designed for residential use and exhibit considerable variation in size, with total net floor areas ranging from 67 m^2 to 155 m^2 and a combined living space of 850 m^2 (970 m^2 gross area), as well as differences in roof types. During the modelling phase of the buildings, limited monitored data was available. As a result, the building models may not fully represent actual performance. Nevertheless, the models were developed mainly based on data obtained during the project development phase. However, for the research purposes in this paper, the energy systems and their setpoints were modified and the obtained data from BPS were used for the paper analysis. Each building has unique thermal characteristics and HVAC system configurations tailor to their design purposes. In the existing arrangement, all buildings are equipped with heat pumps, some have specific designs to achieve passive heating and/or cooling. In this research, each building's HVAC was considered as a reversible air source heat pump with a thermal size of 10 kW and coefficient of performance (COP) of 4.4. The calculated space heating demand is 61 kWh/m^2 per year in the cluster. Additionally, the energy system of each building was modelled with two separate thermal storage tanks, each with a capacity of 500 L (for increased flexibility) —one designated for hot water, which is utilised for both space heating and domestic hot water, and one for cold water storage. The supply temperature for hot water utilised in space heating was modulated according to an ambient temperature-dependent heating curve (HC). Domestic hot water was charged for two hours during the day at a fixed 55°C temperature. The indoor temperature setpoints were established at 21 °C during the heating season and 25 °C during the cooling season. Certain houses were equipped with ceiling radiant heating systems, whereas others were fitted with floor radiant heating systems to serve as their primary heating and cooling room units. The indoor CO_2 level was maintained in the range of 400 ppm to 1000 ppm through mechanical ventilation in two buildings, while the remaining six buildings were ventilated naturally using automated window control. Each house also has its own PV panels with different orientations but a capacity of 2.5 kWp. No electrical energy storage systems were modelled in this research.

Each building had a distinct electrical load profile derived from lighting, equipment, and plug-in loads, in addition to the HVAC system demand. These profiles were correlated with a unique occupancy schedule. The cluster energy model was developed in a BPS tool where the actual recorded weather data for Wuppertal, Germany (by a local weather station) over an entire year is used. The energy model of the cluster, representing the baseline case (signal-unaware scenario), was developed with the actual thermal characteristics of each building defined. The calibrated model was obtained by the monitored data as described in [34]. However, the energy plants were modelled as non-electrical systems in the BPS tool to determine the transformer capacity before electrification

Fig. 1. The Wuppertal cluster buildings simulated in this work (Ref: © Sigurd Steinprinz, University Wuppertal).

2.2. Cluster definition – Basel, Switzerland

This building cluster comprises eight single-family terraced houses that were modelled on existing houses located in Basel, Switzerland (Fig. 2). The climate in Basel has moderate winters and summers, with an annual mean temperature of 11.2 °C and a total global solar radiation of 1273 kWh/m^2 per year. The data used was derived from the most recent 15 years (2007–2021) [35]. The total gross floor area is 137 m^2 (net floor area 114 m^2) for each building, which are of solid-wall construction (brick wall, concrete floors/ceilings), without basement and oriented south/north. The top level of the pitched roof is unheated. The building models retain only the geometric form of existing buildings, reflecting their actual physical shape. However, all other modelling parameters were based on assumptions in accordance with the SIA 380/1 standard. Based on the modelling assumption, each house has a heating demand of 38.6 kWh/m^2 (gross floor area per year) according to [36].

For the modelling purposes, a brine-to-water heat pump with a thermal capacity of 15 kW and a COP of 3.5 was used for each building to meet their heating and domestic hot water demands. Each heat pump fed a 300-liter buffer tank and a 200-liter domestic hot water tank (HWT). The heat was emitted via radiators that draw their heat from the buffer tank. The domestic hot water was produced for two hours in the early morning during the whole year. During summer, between the 1st of May and the 15th of September, the heat pump heating function was switched off and, no mechanical cooling was implemented in the cluster. All buildings have roof mounted south-facing PV systems at 40° inclination. Two buildings have a PV-system with a capacity of 1.5 kWp and the other six buildings 3.0 kWp.

Eight unique household electricity load profiles based on 10-minute increments were used [37] and varied between 7.6–23.5 kWh/m^2 per year. The daily occupancy profiles were based on Swiss standard [38] and were customised for each building, alongside daily hot water usage – both apply to all days of the year.

Ventilation was modelled based on a fixed daily window-opening behaviour, with windows opened four times a day for 10 min each as given in the reference [39]. The four ventilation times vary for each building, and they were independent of the ambient temperature. The range of the ventilation times for all buildings was in the morning between 6:50 – 8:20, after lunch between 13:10–14:50 (except of one building: 17:30–17:40), in the early evening between 18:40–20:20 and late in the evening between 21:50–23:20 as given in the supplementary document – Fig. 1. The radiators were switched off during ventilation times; however, the heat pumps continued to charge the buffer tanks if the monitored temperature fell below the setpoint. In midsummer, between the 15th of June and the 15th of August, additional nighttime natural ventilation was provided in the upper rooms between the evening and morning ventilation time in each building. The external blind was activated when the solar radiation on the outer façade exceeds 120 W/m^2 for two buildings and 150 W/m^2 for the other buildings. The building energy models were created using DesignBuilder [40] and simulated using EnergyPlus [41] at 10-minute simulation steps. In Table 1, the key parameters of both clusters are given.

2.3. Building-Grid interaction signals

Sequential BGI signals differ from single or optimized signals by their dynamic prioritization mechanism, as described in Section 1, which activates specific signals based on predefined grid conditions, such as transformer overload, cost or GHG emission. Unlike single-signal approaches, sequential signals aim to balance competing objectives by integrating real-time feedback from the grid into control strategies. This study incorporates a novel sequential signal framework that evaluates the impacts of combining price- or CO_2-driven signals with TCS signals, thus addressing previously unquantified trade-offs between energy flexibility and grid stability.

2.3.1. Price-driven and emissions-driven Building-Grid interaction signal

Day-ahead prices (DAH) (before tax and surcharge) were utilised as the electricity unit price, with data accessible on the ENTSO-E Transparency Platform [42]. Similarly, CO_2eq intensity data was obtained

Table 1
The key parameters of the clusters.

	German building cluster	Swiss building cluster
Area	Ranging from 67 m^2 to 155 m^2 (net) – in total 850 m^2 (net)	137 m^2 (gross) for each building – in total 1080 m^2 (gross)
Heating system	8 reversible heat pumps – each with a thermal capacity of 10 kW and 4.5 COP	8 heat pumps – each with a thermal capacity of 15 kW and 3.5 COP
Cooling system	8 reversible heat pumps and 8 tanks – each with a volume of 500 L	No mechanical cooling
HWT	8 combi tanks – each with a volume of 500 L	8 tanks – each with a volume of 200 L
Buffer tank	No	8 tanks – each with a volume of 300 L
DHW	From HWT	From HWT
PV	2.5 kWp	1.5/3.0 kWp
Space heating demand (Thermal)	61 kWh/m^2	38.6 kWh/m^2
Space cooling demand (Thermal)	26 kWh/m^2	No mechanical cooling
Cluster total peak demand (Electrical)	11.5 kW	13.6 kW

Fig. 2. The Swiss building cluster simulated in this work (Ref: © Monika Hall).

from the Electricity Maps – Data Portal [43]. Both datasets are from 2023 – they are freely accessible and provided in hourly resolution. DAH are announced every day around 12:00 pm and present the dynamic electricity unit prices for the next entire day. For the purposes of this research, it was assumed that the bidding process in the DAH market was successful throughout the year. This assumes that the building is part of an aggregator's portfolio, enabling participation in the DAH market. Utilising this information, the building energy systems were optimised to use economic operation (i.e., objectively minimise operational costs) by controlling building energy systems within specific indoor thermal comfort setpoints. Accessing average emission data before energy price data is not easy. However, there are some studies that conduct forecasts using artificial intelligence technology, allowing such a signal to be used for environmentally friendly operation of the energy system. In this research, the German and Swiss datasets for price and emissions were exploited under the assumption that the datasets are known 24-hours in advance.

2.3.2. Transformer Building-Grid interaction signal

To generate a TCS BGI signal, a transformer model developed using IEC 60076–7 standard [30] was used in this study. The transformer's rated power was obtained by considering the peak cluster load observed over a year, before the use of available energy flexibility to modify the buildings' load according to the considered BGI signals. In practical applications, transformer design typically includes a security factor above the peak expected load to ensure operational safety. However, in this study, the transformer capacity was intentionally set equal to the peak load of the building cluster, without an additional safety margin. By not incorporating a built-in safety margin, the model exposes the transformer to its full load potential, thereby enabling a more sensitive evaluation of how BGI signals influence transformer heating, aging, and overloading. Since all control strategies and simulations were benchmarked using the same transformer capacity across cases in the specific cluster, the relative differences in aging and critical status are internally consistent and valid for comparison. Although absolute aging values might vary with a different transformer sizing strategy, the observed trends and relative performance of BGI signals remain robust.

The broader district typically consists of a large number of buildings (e.g. more than 50) that are connected to a shared transformer. However, for the purpose of this research, we focused on a smaller representative cluster of eight buildings in to balance computational complexity with a realistic level of detail. While in practice, a transformer would not be dedicated solely to this limited number of buildings; we scaled the transformer size in our models to match the aggregated peak demand of the simulated cluster under baseline conditions. This approach allowed us to isolate the impact of BGI signals on transformer performance under computationally manageable conditions. This resulting transformer capacity is therefore hypothetical, yet aligned with the actual load profile of the selected buildings.

The yearly power demand of the cluster is output at one minute resolution by the BPS tool. The highest demand value was found to be 11.5 kW and 13.6 for the German and Swiss building cluster, respectively which was used as the transformer capacity for the simulation scenarios executed in this research. It is important to note that a distribution transformer in real operation would have higher rated power values, for that reason, the model used based on IEC 60076–7 standard considers the load factor, i.e., absolute load normalised to the rated power, and not the absolute load.

This sizing approach allows future increases in peak load (e.g., resulting from increasing electrification and integration of PV systems) as the transformer does not operate above nominal power during the baseline scenario. At a constant transformer HST of 110 °C, the lifetime of a transformer is specified as 180,000 h, which corresponds to approximately 20.5 years. Since the transformer HST varies depending on the transformer utilisation and the ambient temperature, this must be calculated for each time step. If the transformer HST in the time step is lower than 110 °C, the lifetime is extended; if it is higher, it is shortened. This results in equivalent aging days. A higher number of equivalent aging days corresponds to a faster transformer aging.

The method from IEC 60076–7 was used to calculate the transformer HST and transformer aging. In [24], the standardised method according to IEC 60076–7, for calculating the transformer HST and equivalent aging based on one minute time steps was presented as a difference equation.

In this research, when the transformer HST exceeded 110 °C, TCS BGI signal was switched from zero to one (inactive to active). When this BGI signal became active, it suspended the price or CO_2eq intensity driven operation. More information about the utilisation of these signals is provided in Section 2.4.

2.4. Simulation scenarios

Two single BGI signals, specifically, DAH (€/kWh) and CO_2eq intensity (gCO_2eq/kWh) were used in the building simulations, as described in Section 2.3.1. To conduct the sequential signal analysis, each of these two signals were paired separately with a TCS signal (given in Section 2.3.2) in order to consider the transformer HST. This way it is possible to also evaluate the impact of these signals on building and power grid operation. In total, five different operation simulation scenarios were developed for each of the building clusters as presented in Fig. 3.

The baseline case of a cluster – the REF case was simulated as a reference scenario (no BGI load management is applied) to compare to BGI cases. In the single BGI signal cases, DAH (the DAH case) and CO_2eq intensity signals (the CO_2 case) were used to perform economic and environmental operation, respectively. Their impact on the power grid operation was analysed separately by incorporating TCS BGI signal in the DAH_TR case "DAH and transformer critical status" and "electricity CO_2eq intensity and transformer critical status" in the CO_2_TR case. More information about the utilisation of DAH, electricity CO_2eq intensity and TCS signals as drivers of the cluster control strategies are given in Section 2.5.

2.5. Building cluster control strategies

The basic assumption for the BGI is that a building operates in an economical or environmental-friendly manner. In this way, power demand is used to a greater extent when DAH or GHG emissions are low, or 'favourable'; conversely, higher or 'unfavourable' BGI signal values would trigger reduced demand. To define the 'favourable' and 'unfavourable' hours, an interquartile analysis was applied to categorise the signals for each day. This resulted in, six hours of low (favourable), six hours of high (unfavourable) and 12 h of medium (nominal) signal

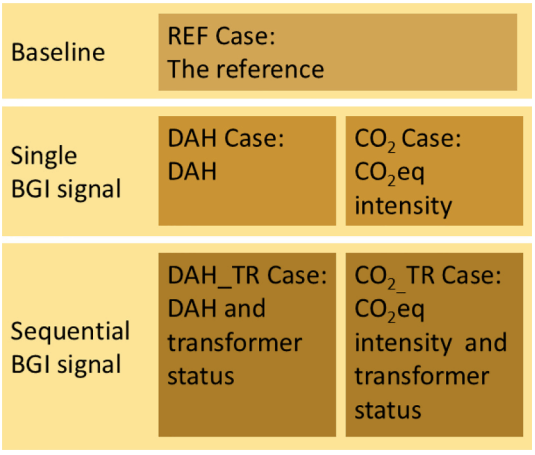

Fig. 3. The simulation cases performed in this research.

categories being established. This process was repeated for each simulation day based on the new daily BGI signal values. During low signal periods (≤ 25 % daily quartile), DAH and CO_2eq intensity are more favourable, allowing the building to operate at a lower cost or in a more environmentally friendly manner compared to the nominal operation. Conversely, during high signal periods (≥ 75 % daily quartile), prices and emissions are at their peak, leading to more expensive or less environmentally friendly building operation. Similar methodology was applied in the previous researches [16,44,45]. The illustration of price categorization using quartile analysis for an example date is included in the supplementary document – Fig. 2. Within the examined cases, ensuring thermal comfort remains a primary constraint at the building level.

In this framework, the control strategies were established based on the defined signal categories and rule-based control was implemented. In the German building cluster, the temperature of the hot and cold water storage tanks were controlled, whilst in the Swiss building cluster the temperatures of the indoor air, buffer and domestic hot water tanks were directly controlled. This approach indirectly manipulated the operation of the heat pump in both cases. It was assumed that all houses in the clusters receive the same signal simultaneously and reacted homogenously. During low (favourable) operating periods, the buildings were thermally charged by increasing the setpoints during the heating period. When the BGI signal entered the high (unfavourable) category, the setpoints were adjusted to slightly lower temperatures to reduce costs/emissions. During medium (nominal) operating periods, the setpoints remained at the same level as in the REF case. It should be noted that in the German building cluster, the heat pumps operated during the cooling season with setpoints adjusted using a similar methodology. However, in the Swiss building cluster, no active BGI signal was applied during the cooling season as there is no mechanical cooling operation.

Table 2 shows the heating season setpoints for the indoor air temperature and the HWT for both clusters respectively. Only the space heating buffer tanks and domestic hot water tank in the Swiss building cluster had direct setpoint temperature control. In the German building cluster, a HC (responding to the ambient temperature) determined the HWT setpoint temperature. Depending on the BGI signal, the temperatures were set to different levels, whereby the medium (nominal) setpoint temperatures were the standard HC values of the REF case operation. In low and high BGI signal periods, the setpoint was increased or reduced, respectively, by 5 °C than the HC value applied in the REF case. In cooling season, the cold-water tank was charged by 5 °C lower and 5 °C higher compared to the REF case cooling curve temperatures, when the BGI signal was at low and high level, respectively. Domestic hot water was charged for two hours during the day at a fixed 55°C temperature, and BGI strategies were not applied to its operation. Prior BPS studies for the German building cluster showed that the indoor temperature was maintained between 21 °C and 25 °C within this HWT temperature ranges. Therefore, there was no additional control strategy applied to retain indoor temperatures. In the Swiss building cluster, the indoor air temperatures were directly controlled based on the BGI signal, e.g. 23 °C and 18 °C were assigned during low and high BGI signal periods, respectively. When the BGI signal was at medium (nominal) levels, 21 °C was applied as in the REF case. If a setpoint of 23 °C was required, more heat from the buffer tank was used to supply the radiators and the buffer tank temperature increased from 50 °C to 55 °C. If the setpoint was at 18 °C, then, the buffer tank set point was set to 40 °C. Additionally, in the Swiss case, domestic hot water was supplied from the HWT. If the charging time coincided with a high BGI signal period, the setpoint was set to 45 °C; otherwise, it remained at 55 °C.

During price- and emission-driven BGI operation, rebound effects may increase stress on the transformer. For example, transformer HST can reach 110 °C when the applied setpoint temperature leads to higher peak loads from the power grid. It Is crucial for the control strategies to be adjusted to resolve the critical status on the transformer as presented in Fig. 4.

In this event, price- and emission-driven BGI operation was overridden, and transformer management took priority. To allow the transformer to cool down after the maximum temperature of 110 °C had been exceeded, the HWT temperature in the German building cluster was set to 10 °C lower than the HC temperature. In the Swiss building cluster, the heat pumps were switched off until the transformer temperature cooled down to a certain temperature. As there is no definition of a lower boundary for the transformer HST, 90 °C was assumed as the lower limit in this research. Occupant comfort was considered a priority, and so the "off" status remained until this hard limit was reached. Therefore, a minimum room temperature of 19 °C and 18 °C must be maintained for the German and Swiss building clusters, respectively.

It should be noted that, in the Swiss building cluster model, the transformer manager had no access to room or tank temperature data, nor to BGI signals. It sent a request to switch off the heat pumps when the transformer temperature was too high. The individual houses complied by adjusting their heating setpoint temperatures to the TCS levels, and the heat pumps were turned off individually if this revised thermal comfort requirement was met.

2.6. Co-simulation environment

In this research, two distinct simulation approaches were performed, each utilising specialised tools designed to meet specific requirements. The simulation approaches both comprise two main steps: (1) the computation of the transformer HST in order to generate a TCS BGI signal and (2) the determination of building performance metrics, such as HVAC operation values and thermal comfort levels. Step (1) was implemented by numerical computing tool and for step (2), BPS tool was utilized. These signals are crucial for implementing control algorithms aimed at demand optimization and for calculating yearly transformer aging. To ensure accuracy, these calculations must be performed concurrently, as each time step's results depend on the preceding step within this dynamic computational framework. To address this challenge, a co-simulation framework was established as per Fig. 5, enabling an in-depth analysis of different BGI signals.

Since this study was conducted through collaboration between two

Table 2
The applied setpoint control strategies for both clusters during heating and cooling seasons. GER: Germany, CH: Switzerland, HS: Heating Season, CS: Cooling Season, HC: Heating Curve, HWT: Hot Water Tank, TCS: Transformer Critical Status.

BGI signal	Cluster GER		Cluster CH		Buffer Tank Cluster GER	Cluster CH	HWT Cluster GER	Cluster CH
	HS	CS	HS	CS				
Baseline	21 °C	25 °C	21 °C	–	–	50 °C	HC	55 °C
Low level DAH/CO_2eq	21 °C	25 °C	23 °C	–	–	55 °C	HC + 5°C	55 °C
Medium level DAH/CO_2eq	21 °C	25 °C	21 °C	–	–	50 °C	HC	55 °C
High level DAH/CO_2eq	21 °C	25 °C	18 °C	–	–	40 °C	HC − 5 °C	45 °C
TCS	If TCS = 1, 19 °C		If TCS = 1, 18 °C		–	If TCS = 1, 40 °C	If TCS = 1, HC − 10 °C	If TCS = 1, 45 °C

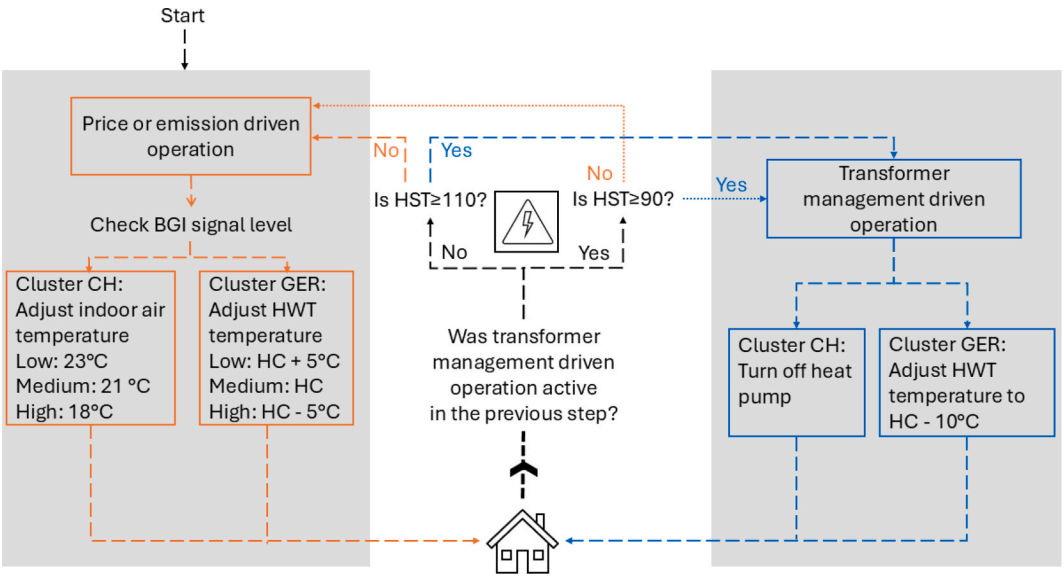

Fig. 4. The operational changes based on the sequential BGI signals in a building cluster. The orange line presents the operation flow described for the DAH case and the CO_2 case. The dynamic interaction with the transformer status is integrated with blue line in the DAH_TR case and the CO_2_TR case. HC: Heating Curve, HST: Hot Spot Temperature, HWT: Hot Water Tank.

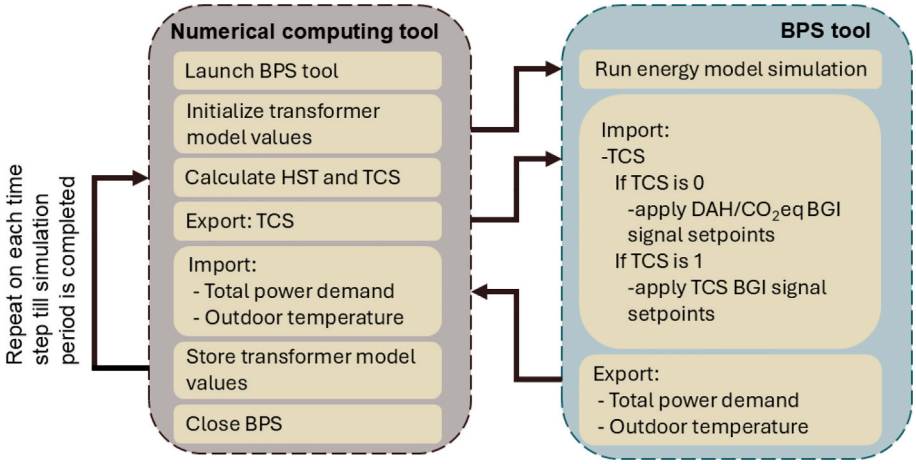

Fig. 5. The workflow between numerical computing tool and BPS tool in co-simulation environment.

institutions, one based in Germany and the other in Switzerland, each team employed the BPS tool standard to their institutional practices. Specifically, this study used a co-simulation environment that integrates BPS tools IDA-ICE [33] and EnergyPlus with numerical computing tools, Matlab [46] and Python [47] in the German and Swiss building cluster, respectively. In German building cluster, the co-simulation environment was established using communication channel as the data exchange pathway in Functional Mock-up Interface, and the Mosaik platform [48] was used in the Swiss building cluster. The time step for the transformer model described in Section 2.3.2 was set to one minute for calculation, as standard practices from IEC 60076–7 suggest this high resolution to accurately mode the thermal phenomena in the internal components of the transformer (e.g., windings temperature variation). In the German building cluster, the co-simulation environment was set up with a 1-minute time step to align with the given standard.

On the other side, this high-resolution calculation resulted in long simulation times and increased computational burden. As a solution to decrease the simulation time, the Swiss institution applied a modified method for calculating the transformer HST, accordingly. The differential equations were reformulated as integrals to enable a more flexible calculation across varying time steps and the simulation time step in the Swiss building cluster was set to 10 min. For verification purposes, the results were compared, showing a close agreement. The deviation of the predicted value of the modified method compared with the standardised method is approximately + 0.2 % for the maximum transformer temperature and approximately + 2 % for aging between the standard method at a 1 min time step, and the modified approach at a 10 min time step [49]. In the supplementary document, Fig. 3 presents the numerical difference between the standard method and modified method. In

Table 3
The used tools and parameters in this research.

	BPS Tool	Numerical Tool	Co-simulation environment	Co-simulation time step
German building cluster	IDA-ICE	Matlab	Channel connection	1 min
Swiss building cluster	EnergyPlus	Python	Mosaik	10 min

Table 3, the tools and parameters to set the co-simulation environment for the clusters are shown.

The objective of using a 1 min or adapted 10 min resolution in the co-simulation is to align with the transformer HST calculation time step. If the time steps of the two tools – namely, the numerical computing tool and the BPS tool – do not align, communication issues may arise, potentially resulting in failure of the co-simulation environment. Moreover, using larger time steps in the BPS tool, such as 30 min or one hour, can lead to missed peak loads, as the tool would compute results based on averaged data over the larger interval, also resulting in limitations for the transformer thermal model due to larger than expected time constants. This, in turn, could result in incorrect estimation of transformer stress.

3. Results

This section presents the simulation results for the two building clusters, evaluating how the same BGI signals influence building and grid operations under distinct operational conditions. Rather than conducting a direct comparison between clusters, this study aims to demonstrate how BGI signals interact with different building characteristics and control strategies. The findings provide insights into the adaptability of sequential BGI signals across varying grid and building contexts.

3.1. Daily load profile under different simulation cases

This section analyses representative daily load profiles from both clusters to illustrate demand variations across different simulation cases. Fig. 6 illustrates the operational demand and transformer state for the German building cluster on the 22nd of January at one minute resolution where the TCS BGI signal for the heating season was observed for the first time. The figure displays the REF case, economic optimisation the DAH case, and economic optimisation with TCS DAH_TR case in subplots A, B, and C, respectively. Since the analysis results exhibit a similar overall profile, the remaining cases – CO_2 and CO_2_TR – are not included in the figure. However, their impacts on transformer operation and other cluster metrics are presented in the next sections. In these three subplots, the cluster power demand, heat pump power demand and PV generation in kW are given on the left axis. The cluster power demand includes all the loads from building cluster, namely the heat pump power demand and baseloads as lighting, equipment, and plug-in loads. In the right axis, transformer HST (°C) and transformer utilisation (%) are illustrated by the dotted lines. In Fig. 6-D, the price BGI signal is

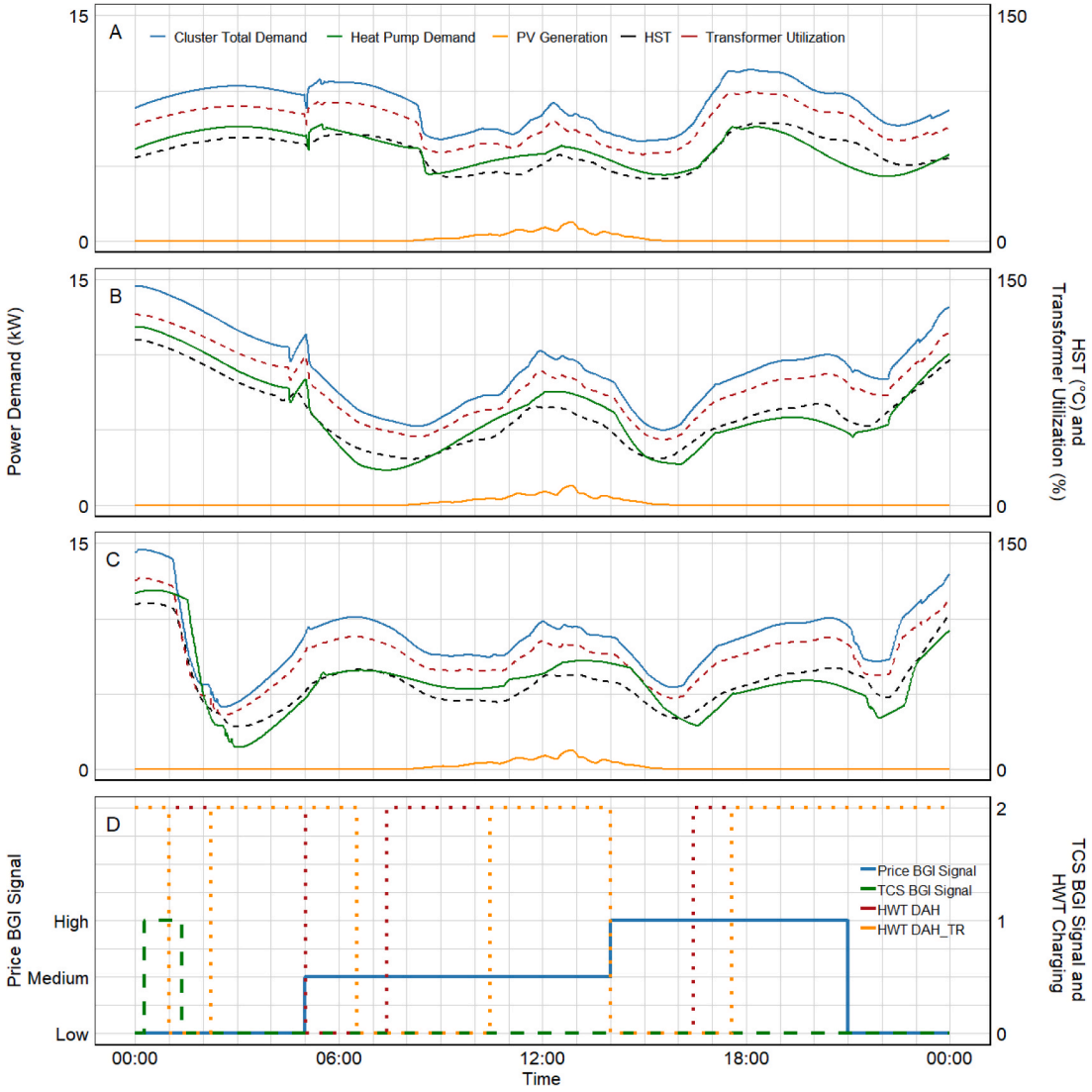

Fig. 6. The daily load profile presentation of the German building cluster for a day in January. Subplots A, B and C present the results from the REF case, the DAH case and the DAH_TR case, respectively. HST: Hot Spot Temperature, HWT: Hot Water Tank, TCS: Transformer Critical Status.

given on the left axis in high, medium and low levels where TCS and HWT charging signals are presented on the right axis. TCS status is defined as 0 (not active) and 1 (active), while HWT charging signal is 0 (no charge) and 2 (charge) on the right axis. The same price signal is exploited in both the DAH case and the DAH_TR case, however, the HWT charging signal varies for these cases since the operation control is in response to the HWT temperature value in addition to the price signal, thus it is presented as HWT DAH case and HWT DAH_TR case. TCS is only introduced for the DAH_TR case as described in Section 2.4. In the REF case, the operation of the heat pumps in the cluster was controlled relative to the ambient temperature HC as baseline operation scenario and the heat pump power demand was the main actor of the total cluster consumption. The highest heat pump and cluster total demand for this representative day were 8.0 kW and 11.5 kW, respectively. The transformer utilisation remained under 100 %, with the transformer HST reaching a safe level of up to 80 °C. Between 08:00 and 14:00, there was a slightly higher PV generation, but as there was no additional control strategy for PV generation in this research, the generation profile was same for all given cases. In Fig. 6-B, the DAH case results showed that, with the price driven strategy, the cumulative demand of eight heat pumps increased to 12 kW when the price was at low level at 00:00 and correspondingly the cluster total demand reached 15 kW. The transformer capacity in the German building cluster was limited to 11.5 kW and during thermal charging of the HWTs, the transformer HST increased to 115 °C, corresponding to a transformer utilisation of 125 %, exceeding its rated capacity. However, since the TCS BGI signal was not implemented in the DAH case, no additional control strategies were available to address the transformer overload when transformer HST reached 110 °C. As the HWT temperature reached the charging setpoint value, the heat pump power demand decreased and, based on the dynamic setpoint varying with the ambient temperature together with price level, the thermal charging was activated during the day at different times as 07:00 and 16:30. If the HWT temperature value was below the setpoint, even though it was a high price event period, e.g. 16:30–21:00, the heat pumps operation continued to ensure thermal comfort.

For the DAH_TR case, to keep the transformer HST below the desired maximum value of 110 °C, the TCS BGI signal was introduced in addition to the price BGI signal in the cluster control strategy. The first low price period started at 00:00 and the power demand of all heat pumps rapidly reached to 11 kW inducing the transformer HST increase (Fig. 6-C). However, when transformer HST raised to 110 °C, the TCS switched from 0 to 1 between 00:15 and 01:20 as given in Fig. 6-D. This event immediately supressed the thermal charging of HWT, and heat pumps' power demand decreased till the transformer HST drops to 90 °C. After ensuring the transformer HST was at 90 °C, the heat pumps again

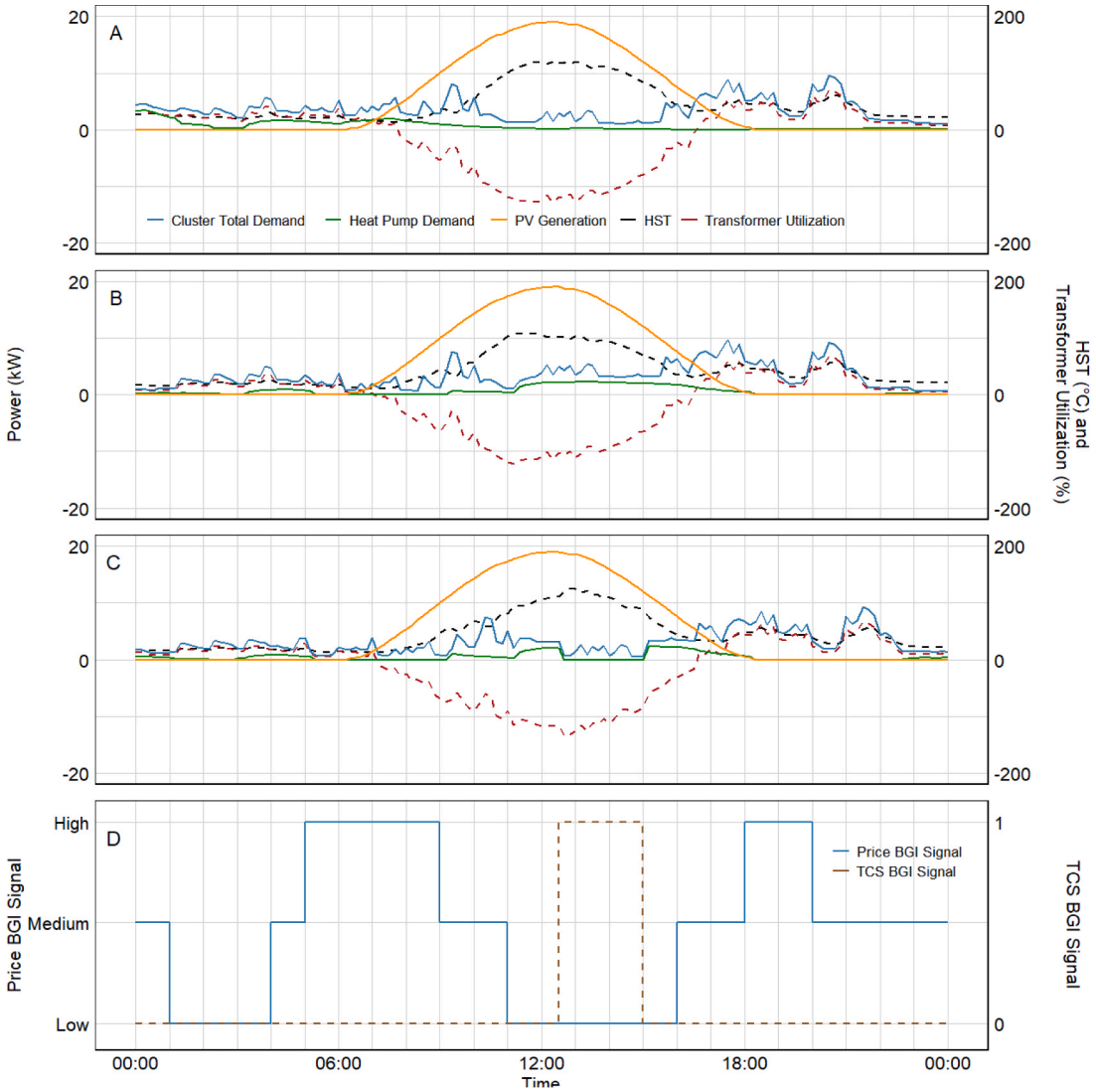

Fig. 7. The daily load profile presentation of the Swiss building cluster for a day in April. Subplots A, B and C present the results from the REF case, the DAH case and the DAH_TR case, respectively. HST: Hot Spot Temperature, TCS: Transformer Critical Status.

charged the HWTs based on the dynamic setpoint value at that certain moment. By falling 20 °C less than the critical transformer HST value, a secured time was ensured to avoid a repetitive TCS event since the following heat pump operation occurred in a short time if the HWT temperature was lower than the charging setpoint. The delayed activation of the HWT charging, kept the transformer HST at a normal range, thus, avoids the rapid transformer aging. This analysis is discussed in Section 3.2.

The operational analysis of the Swiss building cluster under different load management scenarios – REF, DAH, and DAH_TR cases – are presented in Fig. 7 (A), (B), and (C), respectively, using the 7th of April as a representative day.

This date was selected as it marks the first occurrence of the TCS BGI signal during the year. In contrast, in the German building cluster, the first occurrence of the TCS BGI signal (22nd of January) took place on a different day due to differences in climatic conditions, building thermal properties, and control strategies. Since the objective of this study is not to compare the clusters directly but to demonstrate how the operational scenarios apply under different conditions, each cluster was analysed based on the first occurrence of the TCS BGI signal within its respective operational context. This approach ensures that the analysis remains consistent with the goal of evaluating BGI signal utilization across diverse building configurations rather than drawing direct comparisons between clusters.

The Swiss building cluster total demand represents all loads from the entire cluster, including heat pumps as well as baseloads such as lighting, equipment, and plug-in loads. In Fig. 7-D, the price BGI signal and TCS BGI signal are presented. Unlike in the German building cluster, heat pump operation in this case was controlled by the manipulated indoor and buffer tank temperature. Consequently, no HWT thermal charging signal is designated in Fig. 7-D. In Fig. 7-A, which presents the operational analysis for the REF case, the power demand for heat pumps remained low, indicating that most of the cluster total demand was attributed to household loads. The peak heat pump demand and cluster total demand were approximately 3 kW and 10 kW, respectively. Given that PV generation significantly exceeds the total power demand, transformer utilisation was surpassed due to feed-in to the power grid, for instance, exceeding −120 % at 12:00. Consequently, the transformer HST surpassed 100 °C.

The results of the DAH case are presented in Fig. 7-B. As the price fell into the low category around 11:00 (as shown in Fig. 7-D), the indoor and the buffer tank setpoint temperatures raised, leading to an increased power demand from the heat pumps. The cluster total demand, including the additional heat pump demand, was covered by PV generation and the residual load was reduced, which resulted in a slight reduction in transformer utilisation, i.e. −110 %, and transformer HST.

The results of the DAH_TR case are presented in Fig. 7-C. As the transformer HST exceeded 110 °C after 12:00, the TCS switched to 1 (Fig. 7-D), and consequently, electricity consumption by the heat pumps dropped to 0 as they were switched off. However, PV generation remained high, and due to the reduced self-consumption after the heat pumps were deactivated, grid feed-in increased. This, in turn, raised transformer utilisation and further increased the transformer HST. To reduce the transformer HST, the heat pumps need to be activated at midday when there is a high PV surplus in order to increase self-consumption. As the transformer HST must first go down to 90 °C before the heat pumps are allowed to start again, an event extends over a longer period, e.g. two hours. This results in a counterproductive outcome, where the control strategy in the DAH_TR case inadvertently exacerbates transformer loading. This issue is further discussed in Section 4. Fig. 7-B shows that during low prices at midday, the heat pumps are activated with higher indoor setpoint temperatures. In the REF case, only medium target temperatures were set, resulting in a lower electricity demand for space heating than the DAH case.

3.2. Transformer hot spot temperature and aging

The fluctuations in transformer HST across different representative weeks are illustrated in Fig. 8, highlighting the transformer HST peaks. Representative weeks from January (when first TCS BGI signal occurs) and July are given for the German building cluster, whereas weeks from April (when first TCS BGI signal occurs) and July are shown for the Swiss building cluster.

In the heating season, the control of HWT setpoint temperatures in response to the single BGI signals in the German building cluster resulted in a broader range of transformer HST values in January compared to the REF case. For example, the transformer HST varied between 20 °C and 110 °C, whereas in the REF case, it reached up to 80 °C. The broadened setpoint temperatures altered heat pump operation, leading to changes in power demand from the grid. During the cooling season in July, some transformer HST peaks were higher in the REF case since PV generation partially covered the power demand of the building, and the rest was fed into the power grid. In the DAH case and the DAH_TR case, the setpoint of the cold-water storage tank was lower during the favourable BGI signal periods, thereby increasing demand and reducing the surplus electricity feed-in by covering the increased heat pump demand. This leaded to a decreased transformer HST since the transformer stress was mitigated. In some events, transformer HST was higher than the desired maximum value of 110 °C such as 125 °C which occurred a few times due to the feed-in from surplus PV generation. One such event spans the period during which the transformer HST rises above 110 °C and subsequently returns to 90 °C, with the duration of these events varying. Except the feed-in event times, the transformer stress was less in the German building cluster during cooling season because the feed-in was decreased with BGI control strategies exploited by increased active cooling.

As presented in Section 3.1, the transformer was stressed due to PV feed-in event in the Swiss building cluster. In the Swiss building cluster during April, higher transformer HST occurred during midday when feed-in was at its peak. On the 7th of April, the transformer HST value reached 110 °C in the REF case, and when TCS was introduced in the DAH_TR case, the heat pump operation was suspended which lowered the self-consumption and caused higher transformer HST. In the cooling season, there was no mechanical cooling as described in Section 2.2, thus, the transformer HST values remained the same for the cooling season in all cases. Feed-in from the PV generation was the main driver that the transformer HST reached to 130 °C in July.

The transformer aging results, relative to the reference scenario, are presented in Fig. 9. To provide a standardized reference for comparison of transformer aging the overall annual value of the REF case transformer aging was normalized to 100 % as can be seen for the German building cluster in Fig. 9-A and Swiss building cluster in Fig. 9-B. The normalization allows us to compare the transformer aging of the different cases easier.

In the REF case of the German building cluster, where no BGI signal was applied, transformer aging was the lowest at 1.9 days. In this baseline case, the cluster power demand did not have sharp peaks that the transformer capacity was approached frequently. However, when a single BGI signal was used, such as in the DAH case and CO_2 case, the applied control strategy caused significant peaks resulting in reaching to the transformer capacity, where faster transformer aging ensued.

The most rapid aging occurred in the DAH case and then following in the CO_2 case with slightly less difference as 262 % and 253 %, respectively. When the TCS signal was included in the DAH_TR case and the CO_2_TR case, the building energy systems operation could align with the transformer needs, e.g., the cluster's power demand was reduced, alleviating transformer stress. As seen, by the introduction of this signal, the relative aging was found lower as 250 % and 230 % in the DAH_TR case and CO2_TR case compared to the CO_2 and DAH cases, respectively. The rapid aging during heating season addresses the impact of demand peak developments from BGI control strategies, e.g., applying higher

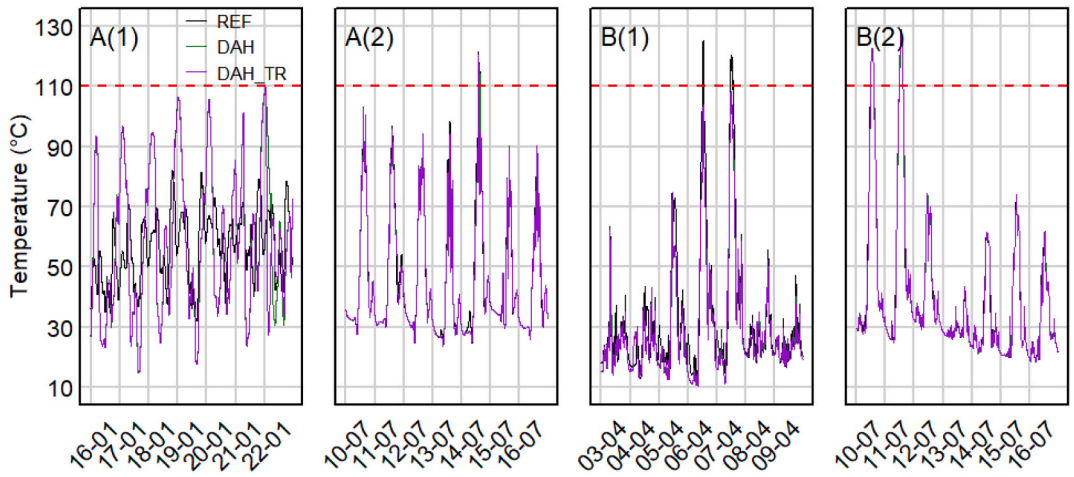

Fig. 8. The transformer HST change for the selected cases for representative weeks, where the red line represents the HST limit which triggers a TCS BGI signal. A(1) and A(2) present the results from the German building cluster, whereas B(1) and B(2) show the results for the Swiss building cluster.

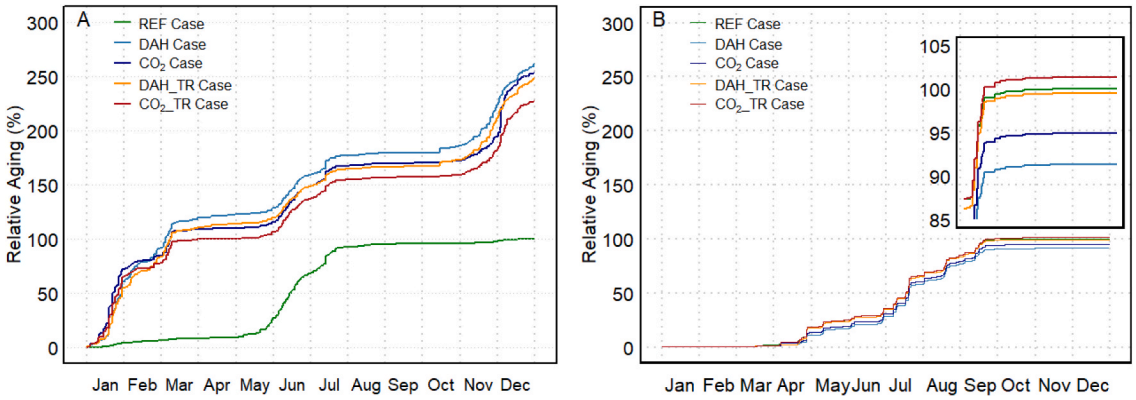

Fig. 9. The transformer relative aging for both clusters over a year. A – German building cluster, B-Swiss building cluster. The Swiss building cluster relative aging between September and December is illustrated in a zoom view.

setpoints compared to the REF case. In the cooling season, PV generation was at the highest level where it covered mainly the cooling demand. Besides, when there was relatively less demand and surplus generation, it was fed into the power grid. As seen during June and July, the aging accelerated where the feed-in caused higher transformer HST in all cases. During the transition season, i.e., May and September, the building heating and cooling demands were lower, hereby, BGI control could not take place often as applied during the rest of the year.

In the Swiss building cluster, the equivalent aging days in the REF case is 16.7 due to PV feed-in. The PV feed-in in the German building cluster is relatively lower compared to the Swiss building cluster. Therefore, there is a significant difference in transformer aging between the two clusters. In general, the single BGI signal operations in the DAH case and CO_2 case showed the lowest relative aging as 91 % and 95 %, respectively (Fig. 9-B). In those cases, the heat pumps often ran around midday during the heating season, when PV yield was also available. This increased the self-sufficiency and reduced the grid feed-in, which had a positive influence on aging. In the DAH_TR case and the CO_2_TR case, since the TCS BGI signal was rarely activated, they showed almost the same aging curve as 99 % and 101 %, respectively. As the main aging took place in summer due to the high grid feed-in the aging of all Swiss building cluster cases were close. The impact of PV feed-in is evaluated more in the Discussion section.

3.3. Transformer load, cost, greenhouse gas emissions and thermal comfort change

The cases DAH, CO_2, DAH_TR and CO_2_TR, where BGI signal were exploited in the cluster operation, were compared to the baseline operation – the REF case. The analysis under different operation scenarios revealed distinct results between the two building clusters located in Germany and Switzerland. In Fig. 10, the transformer load observed at the power grid meter connected to the transformer is shown, reflecting values after accounting for self-consumption.

In the German building cluster, transformer load increased in the range of 6.0 % to 7.1 % when BGI control strategies were applied. In the single BGI signal operation, the transformer load was slightly lower than sequential BGI signal cases. In the Swiss building cluster, the transformer load increased in the DAH case and the DAH_TR case in the range of 2.6 % to 2.8 % where price BGI signal was used in the cluster operation. However, in the CO_2 case and the CO_2_TR case –where CO_2eq intensity BGI signal was utilised- transformer load decreased 0.9 % because CO_2eq intensities changed very often and rarely longer periods with high or low setpoints occur. Since TCS BGI for CO_2eq. was more rarely activated than the DAH cases, no change was observed between the CO_2 case and the CO_2_TR case in the Swiss building cluster.

The cost saving was higher in the DAH case and the DAH_TR case around 4.0 % and 8.0 % for the German and Swiss building clusters respectively, as presented in Fig. 11. Fewer savings in the CO_2 case and CO_2_TR were calculated since the DAH and CO_2eq intensity are not

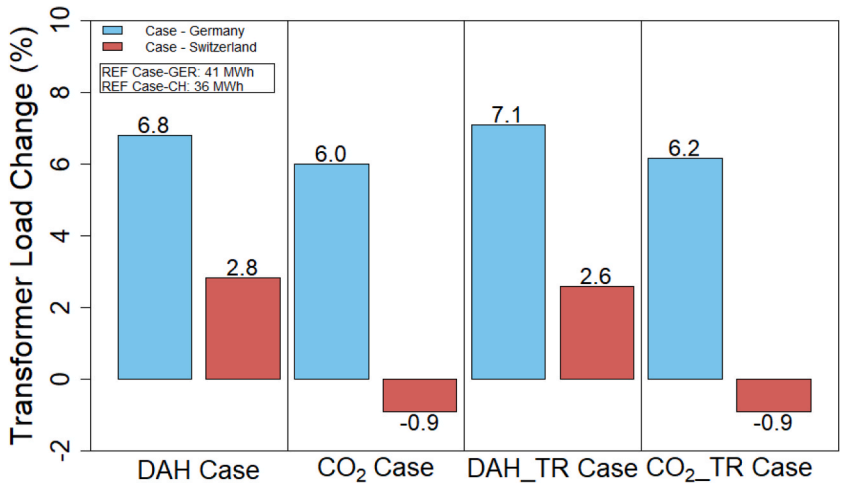

Fig. 10. Yearly transformer load change relative to the REF case for both clusters.

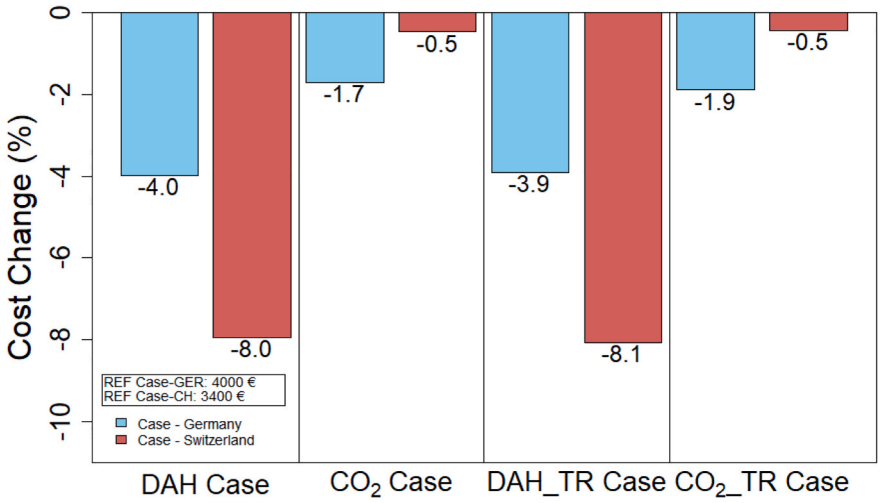

Fig. 11. Yearly energy cost change relative to the REF case for both clusters.

correlated positively among year all the time. When a cluster is operated using a BGI signal with a certain objective, e.g. a price signal to achieve economical saving, this may reflect oppositely on the operational savings of cases where different objective is aimed such as reducing GHG. The results of DAH and DAH_TR case were close to each other on both clusters since the TCS occurred a few times during the year which did not change the operational savings significantly. The same behaviour also was seen for the CO_2 case and the CO_2_TR case. As mentioned above

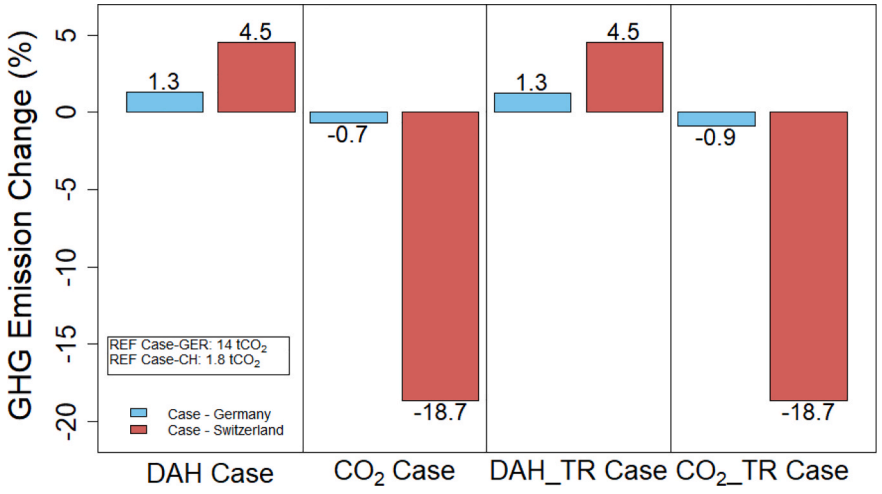

Fig. 12. Yearly GHG emission change relative to the REF case for both clusters.

TCS BGI for CO2eq. was more rarely activated than the DAH cases, no change was observed between the CO_2 case and the CO2_TR case in the Swiss building cluster.

As given in the cost change analysis, the uncorrelated trend of DAH and CO_2eq intensity BGI signal affected GHG emission saving differently on the DAH case and the CO_2 case. In Fig. 12, the GHG emission was 0.7 % less in the CO_2 case compared to the REF case and it was found 0.9 % less in the CO_2_TR case for the German building cluster. In the Swiss building cluster, the GHG emission had a reduction of 18.7 % under the CO_2eq intensity signal operation in the CO_2 case and (5). As described before, TCS occurs rarely, therefore the results were the same or did not differentiate significantly. Conversely, the GHG emissions increased by 1.3 % and 4.5 % in the DAH case and the DAH_TR case for the German and Swiss building cluster, respectively.

The BGI operational control strategies must be implemented without compromising thermal comfort as discussed in Section 2.5. To assess this, the operative temperature of one selected building from the German building cluster (Fig. 13-A) and the Swiss building cluster (Fig. 13-B) under the DAH_TR case operation is presented for the entire year. In German building cluster, active heating and cooling were utilised to maintain indoor temperatures between 21 °C and 25 °C, in alignment with the ISO 7730 standard [50]. In contrast, the Switzerland case lacked mechanical cooling, adhering instead to the comfort range defined by the SIA 180 standard [51]. This standard considers the moving average of the ambient temperature over 48 h as a benchmark for acceptable comfort levels. In both clusters, there were instances where temperatures exceeded or fell short of the prescribed limits: 21 °C in the German building cluster and the SIA 180 limits in the Swiss building cluster. In the German and Swiss building cluster, the lowest indoor temperature for the representative buildings was 20.3 °C and 18.0 °C, respectively. These deviations arose because ventilation, achieved through manual window operation, was controlled either by indoor CO_2 levels or a fixed window opening schedules. In the Swiss building cluster, where the BGI control strategy was limited to heat pump operation during the heating period, deviations below the lower temperature limit for heating were highlighted in the grey area. Nonetheless, temperatures below the lower limit occurred only within a narrow range in both clusters.

Temperatures below the lower limit and above the higher limit occurred during the non-heating season (white area). The shortfalls occurred due to the fix nighttime ventilation between the 15th of June and the 15th of August. The excesses are based on the window opening times during daytime. As mentioned, the ventilation time is based on a fix time schedule and independent of the ambient temperature. Crucially, for both occupant comfort and the effective implementation of this control strategy, thermal conditions were maintained in both clusters. However, slightly lower indoor temperatures were observed due to natural ventilation.

4. Discussion

This research analysed the operation of the building clusters and their transformers over an entire year. Single day building operation results showed distinct differences between the examined building clusters. In the German building cluster, the TCS was triggered due to the increased heat pump demand in the cluster. However, in the Swiss building cluster, the heat pump demand was comparatively less than the overall cluster demand. Especially because of the high amount of PV generation, where the excess power was fed into the grid resulting in transformer overload triggering the TCS. When the transformer is overloaded, in principle, the demand should be reduced. In the Swiss building cluster, reducing demand led to a decrease in PV energy consumption during heating season, which reduced self-sufficiency. Consequently, the amount of power fed into the grid increased. To avoid this situation, we want to highlight the importance of integrating advanced control strategies specific to each building within the cluster. If transformer HST is high due to feed-in, large consumers should adjust their setpoint temperatures to peak values within the acceptable range of thermal comfort levels or switch on their HVAC systems. If no grid feed-in occurs during times with high transformer HST, the building/s with high demand should minimise their demand or switch off their HVAC systems. In this research, all buildings in the same cluster were controlled with the same control strategy and no individual control was applied for each building. Our future work involves developing customized control strategies for each building, aligned to its demand profile.

While the clusters are not meant to be compared in a normative sense (e.g., which performs better), their differences allow us to observe how system behaviour and control outcomes vary due to system-specific properties. For example, in the German building cluster, where the cluster peak heating demand is higher than the Swiss building cluster, the load shifting could be applied on a larger scale. Higher setpoints lead to greater demand on the heat pump and the thermal storage, enabling effective peak shaving during periods of low BGI categories. However, the increased peaks resulted in faster aging during heating season. In contrast, the peak heating demand is lower because of buildings thermal properties in the Swiss building cluster, and the higher setpoints setting did not accelerate the transformer aging on the heating system since the increased heating demand was partially covered by PV generation. Therefore, the aging resulted in a lower value compared to REF case. During the cooling season, the rapid transformer aging was slowed down in the German building cluster as PV generation partially covered the

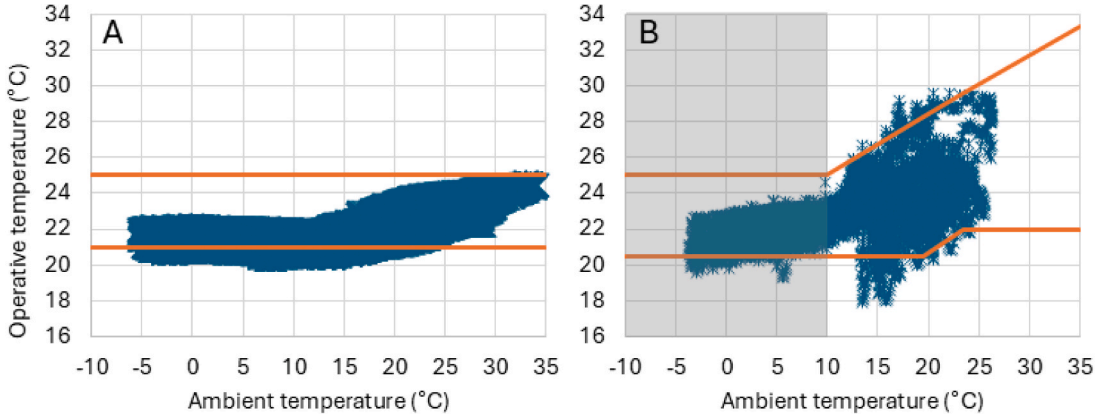

Fig. 13. The indoor operative temperature of representative buildings from the cluster Germany (A) and Switzerland (B). In (A), ISO 7730 standard with fixed temperature boundaries is applied. In (B), the moving average of the ambient temperature over 48 h according to SIA 180 is applied and presented on the x-axis. Grey area in (B) presents the heating season.

cooling demand and there were less feed-in events compared to the REF case. Conversely, the Swiss building cluster's lack of mechanical cooling system limits its summer flexibility, leading to TCS events and fewer opportunities for dynamic control, which results in rapid transformer aging during the cooling season, i.e., the transformer aging was less than REF case in DAH and CO_2 cases. This leads to observable differences in transformer HST profiles and aging rates under the same BGI control structure between clusters. It is important to note that the transformer HST is affected not only by the cumulative cluster power demand, but also by the ambient temperature as previously mentioned. If this research were conducted in a region with vastly different climate characteristics, the TCS could activate more frequently, potentially accelerating the transformer aging and maintenance cost.

When evaluating yearly metrics such as transformer load, cost, and GHG emission savings, no significant differences were observed between DAH and the DAH_TR cases and also between CO_2 and the CO_2_TR cases. However, the timing of peak events during the day differed. This discrepancy arises because the CO_2eq intensity value is not always positively correlated with the price value [29]. In future, when the electricity market dynamic aligns closer with the RES supply and demand imbalances, an integrated strategy can be applied for both cost and GHG emission saving. Although electric vehicles are not examined in this study, their increasing share is expected to influence transformer load. Incorporating charging strategies have to be included in the BGI signal controls.

On the other side, both clusters include highly insulated, energy-efficient buildings. This raises questions about the future viability of building–grid interaction as the stock of energy-efficient buildings grows. When most buildings have minimal heating and cooling demands, their ability to relieve congestion events will be limited, and the resulting cost savings may not be sufficient to motivate end users to participate. Consequently, more innovative business models and incentive structures will be needed to sustain engagement in building-grid interaction schemes.

These variations underscore a key finding: BGI signals perform very differently depending on each cluster's system setup, seasonal operating patterns and flexibility reserves. Rather than aiming for uniform results, our study stresses the importance of fitting control strategies to each scenario and shows how signals can produce varied effects, even when driven by the same protocols, because of each cluster's distinct composition. A key insight from this study is the importance of distinguishing between load-driven and generation-driven transformer stress when designing flexibility control strategies. In load-driven scenarios, such as peak heating or cooling demand, reducing or shifting consumption is a viable means to relieve transformer stress. In contrast, generation-driven stress, e.g., caused by high PV feed-in, requires alternative strategies, such as coordinated load activation or storage integration, to absorb excess generation and avoid back feeding-related transformer overload. Therefore, applying identical control signals across clusters without accounting for the dominant source of transformer stress may lead to suboptimal outcomes. Including two clusters helps to highlight that flexibility solutions are not one-size-fits-all. This is particularly relevant for stakeholders developing scalable demand side management strategies or integrating flexibility into building stock.

Additionally, authors consider three operational control strategies that could be applied as future work: curtailment of PV generation, implementation of an electrical energy storage system and scheduling the preheating of domestic hot water system during high PV generation. The first option provides a complete solution by curtailing generation in proportion to the extent of transformer overloading. In some countries like Germany, this approach is applied. However, this also would mean a reduction in renewable energy usage, which does not align with the transition efforts from fossil-based systems to RES. Charging electrical energy storage systems, electrical vehicles and preheating the domestic hot water storage could assist the power grid operation during feed-in times. This also would increase the self-sufficiency of the system. Additionally, in the case of applying these advanced control strategies, we suggest considering energy sharing solutions within a building cluster where the energy is shared within the local grid. Various business models can be applied that the power is sold to the grid/local network or traded between the neighbours.

5. Conclusion

In this research, we address the growing demand for Building-Grid Interaction (BGI) applications at cluster level which plays a significant role for electrification and full integration of renewable energy systems (RES) into power grid. In this study, single and sequential BGI signals were exploited to unlock energy flexibility and present their impact on the power grid. The single BGI signals used were day-ahead prices and electricity CO_2eq intensity to enable economical and grid-friendly operation in different simulation cases, respectively. To reflect the status of power grids, especially when there is peak shift event occurring during favourable BGI signal times, a transformer model that complies with the IEC 60076–7 standard was integrated into the Building Performance Simulation (BPS) environment and the research was conducted under a co-simulation framework. Two energy-efficient building clusters from Germany and Switzerland, were used as case studies. Since the power grid robustness has priority over the price or the CO_2eq intensity BGI signal operation, a hierarchical approach was applied where TCS BGI signal overrides the in-use BGI signal and changes the operational control strategies in order to support the reliable power grid operation.

The results reveal that while single BGI signal implementation optimise demand side management, their simultaneous application within a cluster can trigger grid instabilities, highlighting the need for additional BGI signal such as TCS. The sequential integration of TCS with other BGI signal effectively prevents transformer overloads. However, the control strategy should be building customized focusing on the transformer stress ground as load-driven or generation-driven transformer. The findings suggest future research on integrating advanced controls and advanced control technologies such as electrical energy storage utilisation and energy-sharing models within a cluster to enhance energy system resilience and flexibility. These outcomes offer strategies for integrating buildings into the power grid and supporting the shift to a low-carbon future.

Another important point the authors want to highlight is the challenges to conduct a BGI analysis in a co-simulation environment. In the market, there are various BPS tools that can be purchased or freely used. During the transition of energy supply systems, the users require a platform where the cluster of buildings and energy grid analysis can be performed together without requiring heavy additional effort. In this research, to carry out the BGI analysis, different tools were coupled, and considerable time was spent to obtain stable communication between the tools and print high resolution data. Moreover, this output data was stored in those tools individually and required additional time for post-processing. With the growing electrification and BGI applications, the demand for user-friendly, fast and stable tools will be increasing.

Declaration of Generative AI and AI-assisted technologies in the writing process

During the preparation of this work the authors used OpenAI ChatGPT in order to improve the readability and language of the manuscript. After using this tool/service, the authors reviewed and edited the content as needed and take full responsibility for the content of the published article.

CRediT authorship contribution statement

Tuğçin Kırant-Mitić: Writing – review & editing, Writing – original draft, Visualization, Validation, Methodology, Formal analysis, Data

curation, Conceptualization. **Monika Hall:** Writing – review & editing, Validation, Methodology, Formal analysis, Data curation, Conceptualization. **George Dawes:** Writing – review & editing, Methodology, Conceptualization. **Rui Amaral Lopes:** Writing – review & editing, Software, Resources, Methodology, Conceptualization.

Declaration of competing interest

The authors declare that they have no known competing financial interests or personal relationships that could have appeared to influence the work reported in this paper.

Acknowledgements

The authors would like to gratefully acknowledge the IEA EBC Annex 82 for providing the framework in which this work was completed. The analysis of the German building cluster in this research was carried out in the framework of the project "Living Lab NRW" supported by the Ministry of Economic Affairs, Industry, Climate Action and Energy of North Rhein-Westphalia under the contract number EFO 0027. The Swiss work described in this paper was funded by the Swiss Federal Office of Energy SFOE under contract number BFE SI/502154. The UK contribution to this work was made possible by support from the EPSRC & SFI Centre for Doctoral Training in Energy Resilience and the Built Environment (ERBE CDT) (grant EP/E21671/1). The Portuguese contributions were supported by the Portuguese "Fundação para a Ciência e a Tecnologia" (FCT) in the context of the Center of Technology and Systems CTS/UNINOVA/FCT/NOVA, reference UIDB/00066/2020.

Appendix A. Supplementary data

Supplementary data to this article can be found online at https://doi.org/10.1016/j.enbuild.2025.116235.

Data availability

Data will be made available on request.

References

[1] United Nations, *The Paris Agreement | United Nations.* [Online]. Available: https://www.un.org/en/climatechange/paris-agreement (accessed: Jul. 21 2024).
[2] C. Peng, J. Zou, L. Lian, Dispatching strategies of electric vehicles participating in frequency regulation on power grid: a review, Renew. Sustain. Energy Rev. 68 (2017) 147–152, https://doi.org/10.1016/j.rser.2016.09.133.
[3] Y. Chen, et al., Experimental investigation of demand response potential of buildings: combined passive thermal mass and active storage, Appl. Energy 280 (2020) 115956, https://doi.org/10.1016/j.apenergy.2020.115956.
[4] W. Liao, F. Xiao, Y. Li, H. Zhang, J. Peng, A comparative study of demand-side energy management strategies for building integrated photovoltaics-battery and electric vehicles (EVs) in diversified building communities, Appl. Energy 361 (2024) 122881, https://doi.org/10.1016/j.apenergy.2024.122881.
[5] D. J. S. Coumans, M. O. W. Grond, and E. J. Coster, "Impacts of future residential electricity demand and storage systems on 'classic' LV-network design," in *2015 IEEE Eindhoven PowerTech*, Eindhoven, Netherlands, 2015, pp. 1–6.
[6] S. Shao, M. Pipattanasomporn, S. Rahman, Demand Response as a load Shaping Tool in an Intelligent Grid with Electric Vehicles, IEEE Trans. Smart Grid 2 (4) (2011) 624–631, https://doi.org/10.1109/TSG.2011.2164583.
[7] P. Hoseinpoori, A.V. Olympios, C.N. Markides, J. Woods, N. Shah, A whole-system approach for quantifying the value of smart electrification for decarbonising heating in buildings, Energ. Conver. Manage. 268 (2022) 115952, https://doi.org/10.1016/j.enconman.2022.115952.
[8] J. Kossahl, J. Kranz, N. Opitz, and L. Kolbe, Eds., *A Perception-based Model for Smart Grid Adoption of Distribution System Operators - An Empirical Analysis*, 2012.
[9] A. Usman, S.H. Shami, Evolution of Communication Technologies for Smart Grid applications, Renew. Sustain. Energy Rev. 19 (2013) 191–199, https://doi.org/10.1016/j.rser.2012.11.002.
[10] F.R. Albogamy, et al., Real-Time Energy Management and load Scheduling with Renewable Energy Integration in Smart Grid, Sustainability 14 (3) (2022) 1792, https://doi.org/10.3390/su14031792.
[11] M.J. Kalani, M. Kalani, Controlling the energy supply and demand of grid-connected building integrated photovoltaics considering real-time electricity prices to develop more sustainable and smarter cities, Optik 300 (2024) 171629, https://doi.org/10.1016/j.ijleo.2024.171629.
[12] European Union Directorate-General, *European Energy Performance of Buildings Directive: Smart readiness indicator.* [Online]. Available: https://energy.ec.europa.eu/topics/energy-efficiency/energy-efficient-buildings/smart-readiness-indicator_en (accessed: 12-Dec-24).
[13] Y.-J. Kim, G. Del-Rosario-Calaf, L.K. Norford, Analysis and Experimental Implementation of Grid Frequency Regulation using Behind-the-Meter Batteries Compensating for Fast load demand Variations, IEEE Trans. Power Syst. 32 (1) (2017) 484–498, https://doi.org/10.1109/TPWRS.2016.2561258.
[14] Y. Ding *et al.*, "Development of a DSO-market on flexibility services," 2013. Accessed: Aug. 2 2024.
[15] Z. Afroz, H. Wu, S. Sethuvenkatraman, G. Henze, R. Grønborg Junker, M. Shepit, A study on price responsive energy flexibility of an office building under cooling dominated climatic conditions, Energ. Buildings 316 (2024) 114359, https://doi.org/10.1016/j.enbuild.2024.114359.
[16] J. Clauß, S. Stinner, C. Solli, K.B. Lindberg, H. Madsen, L. Georges, Evaluation Method for the Hourly Average CO2eq. Intensity of the Electricity Mix and its Application to the demand Response of Residential heating, Energies 12 (7) (2019) 1345, https://doi.org/10.3390/en12071345.
[17] M. You, Q. Wang, H. Sun, I. Castro, J. Jiang, Digital twins based day-ahead integrated energy system scheduling under load and renewable energy uncertainties, Appl. Energy 305 (2022) 117899, https://doi.org/10.1016/j.apenergy.2021.117899.
[18] L. Zheng, B. Zhou, Y. Cao, S. Wing Or, Y. Li, K. Wing Chan, Hierarchical distributed multi-energy demand response for coordinated operation of building clusters, Appl. Energy 308 (2022) 118362, https://doi.org/10.1016/j.apenergy.2021.118362.
[19] N.G. Paterakis, O. Erdinc, I.N. Pappi, A.G. Bakirtzis, J.P.S. Catalao, Coordinated operation of a Neighborhood of Smart Households Comprising Electric Vehicles, Energy Storage and distributed Generation, IEEE Trans. Smart Grid 7 (6) (2016) 2736–2747, https://doi.org/10.1109/TSG.2015.2512501.
[20] R.G. Junker, et al., Characterizing the energy flexibility of buildings and districts, Appl. Energy 225 (2018) 175–182, https://doi.org/10.1016/j.apenergy.2018.05.037.
[21] M. Song, K. Alvehag, J. Widén, A. Parisio, Estimating the impacts of demand response by simulating household behaviours under price and CO2 signals, Electr. Pow. Syst. Res. 111 (2014) 103–114, https://doi.org/10.1016/j.epsr.2014.02.016.
[22] M. Kilthau, et al., Integrating Peer-to-Peer Energy Trading and Flexibility Market with Self-Sovereign Identity for Decentralized Energy Dispatch and Congestion Management, IEEE Access 11 (2023) 145395–145420, https://doi.org/10.1109/ACCESS.2023.3344855.
[23] D. Cano-Tirado, M. Forchheim, M. Asman, M. Zdrallek, and S. Palmer, Eds., *Potential Grid-Oriented and Market-Oriented Optimisation of a Local Charging Infrastructure Through a Genetic Algorithm*. Austria, 2024.
[24] R.A. Lopes, P. Magalhães, J.P. Gouveia, D. Aelenei, C. Lima, J. Martins, A case study on the impact of nearly Zero-Energy buildings on distribution transformer aging, Energy 157 (2018) 669–678, https://doi.org/10.1016/j.energy.2018.05.148.
[25] S. Hussain, M.I. Azim, C. Lai, U. Eicker, New coordination framework for smart home peer-to-peer trading to reduce impact on distribution transformer, Energy 284 (2023) 129297, https://doi.org/10.1016/j.energy.2023.129297.
[26] J. Langevin, et al., Customer enrollment and participation in building demand management programs: a review of key factors, Energ. Buildings 320 (2024) 114618, https://doi.org/10.1016/J.ENBUILD.2024.114618.
[27] A. Nilsson, P. Stoll, N. Brandt, Assessing the impact of real-time price visualization on residential electricity consumption, costs, and carbon emissions, Resour. Conserv. Recycl. 124 (2017) 152–161, https://doi.org/10.1016/j.resconrec.2015.10.007.
[28] Z. Pooranian, J. Abawajy, V. P, and M. Conti, "Scheduling Distributed Energy Resource Operation and Daily Power Consumption for a Smart Building to Optimize Economic and Environmental Parameters," *Energies*, vol. 11, no. 6, p. 1348, 2018, doi: 10.3390/en11061348.
[29] T. Kirant Mitić, K. Voss, Development of a Joint Penalty Signal for Building Energy Flexibility in operation with Power Grids: Analysis and Case Study, Buildings 13 (5) (2023) 1338, https://doi.org/10.3390/buildings13051338.
[30] IEC 60076-7:2005, *Power transformers - Part 7: Loading guide for oil-immersed power transformers*: International Electrotechnical Commission, vol. 29.180. Accessed: 2024. [Online]. Available: https://webstore.iec.ch/en/publication/605.
[31] Solar Decathlon Europe 21/22, *SDE.* [Online]. Available: https://sdeurope.uni-wuppertal.de/de/ (accessed: 15-Aug-23).
[32] K. Voss, I. Kalpkirmaz Rizaoglu, A. Balcerzak, H. Hansen, Solar energy engineering and solar system integration – the solar Decathlon Europe 21/22 student competition experiences, Energ. Buildings 285 (2023) 112891, https://doi.org/10.1016/j.enbuild.2023.112891.
[33] IDA-ICE, *Equa Simulation AB - IDA indoor climate and energy 4.8 - Simulation Software | EQUA.* [Online]. Available: https://www.equa.se/en (accessed: 15-Aug-23).
[34] T. Kırant-Mitić and K. Voss, "Enhancing Grid Stability and Economic Operation through Heuristic Control: A Simulation Case Study," in *Proceedings of BauSim 2024: 10th Conference of IBPSA-Germany and Austria*, 2024.
[35] Lawrie, Linda K, Drury B. Crawley, *Development of Global Typical Meteorological Years (TMYx).* [Online]. Available: https://climate.onebuilding.org/ (accessed: 09-Dec-24).
[36] SIA 380/1, *Heizwärmebedar*. Zürich, Schweiz: Schweizerischer Ingenieur- und Architektenverein. Accessed: 2024. [Online]. Available: https://shop.sia.ch/normenwerk/architekt/380-1_2016_d/D/Product.

[37] N. Pflugradt, *LoadProfileGenerator*. [Online]. Available: https://www.loadprofilegenerator.de/references/ (accessed: 09-Dec-24).
[38] SIA 2024:2021, *Raumnutzungsdaten für die Energie- und Gebäudetechnik*. Zürich, Schweiz: Schweizerischer Ingenieur- und Architektenverein.
[39] EnergieSchweiz, *Suche*. [Online]. Available: https://www.energieschweiz.ch/search/?searchInput=Besser+Wohnen (accessed: 25-Jun-25).
[40] DesignBuilder Software Ltd, *DesignBuilder*, 2002. Accessed: 09-Dec-24. [Online]. Available: https://designbuilder.co.uk/.
[41] National Renewable Energy Laboratory, *EnergyPlus*: The U.S. Department of Energy's Building Technologies Office, 1996. Accessed: 2024. [Online]. Available: https://energyplus.net/.
[42] ENTSO-E Transparency Platform, *Day-ahead Prices*. [Online]. Available: https://transparency.entsoe.eu/dashboard/show (accessed: Dec-2022).
[43] Electricity Maps, *CO_2 emissions of electricity consumption*. [Online]. Available: https://app.electricitymaps.com/map (accessed: 09-Dec-24).
[44] M. Hall, A. Geissler, Comparison of Flexibility Factors and Introduction of a Flexibility Classification using Advanced Heat Pump Control, Energies 14 (24) (2021) 8391, https://doi.org/10.3390/en14248391.
[45] J. Le Dréau, P. Heiselberg, Energy flexibility of residential buildings using short term heat storage in the thermal mass, Energy 111 (2016) 991–1002, https://doi.org/10.1016/j.energy.2016.05.076.
[46] MATLAB, *(R2015b)*. Natick, Massachusetts: The MathWorks Inc, 2015.
[47] Python Software Foundation, *Python*, 2001. Accessed: 2024. [Online]. Available: https://www.python.org/.
[48] C. Steinbrink, et al., CPES Testing with mosaik: Co-simulation Planning, Execution and Analysis, Appl. Sci. 9 (5) (2019) 923, https://doi.org/10.3390/app9050923.
[49] Hall, M., Geissler, A., *FlexiCluster - Energy flexibility of building clusters*. [Online]. Available: https://www.aramis.admin.ch/Grunddaten/?ProjectID=47510.
[50] ISO, *ISO 7730: Ergonomics of the thermal environment: Analytical determination and interpretation of thermal comfort using calculation of the PMV and PPD indices and local thermal comfort criteria*. Geneva.
[51] SIA 180, *Wärmeschutz, Feuchteschutz und Raumklima in Gebäuden*: Schweizerischer Ingenieur- und Architektenverein. [Online]. Available: https://shop.sia.ch/normenwerk/architekt/sia%20180/d/2014/D/Product.